Chinese Journal of Natural Medicines

New pimarane diterpenoids with antibacterial activity from fungus *Arthrinium* sp. ZS03

Songfeng ZHAO, Ziwei JING

Citation: Songfeng ZHAO, Ziwei JING, New pimarane diterpenoids with antibacterial activity from fungus *Arthrinium* sp. ZS03, Chinese Journal of Natural Medicines, 2024, 22(4), 356−364. doi: 10.1016/S1875−5364(24)60629−1.

View online: https://doi.org/10.1016/S1875−5364(24)60629−1

Available online at www.sciencedirect.com
ScienceDirect
Chinese Journal of Natural Medicines 2024, **22**(4): 356-364
doi: 10.1016/S1875-5364(24)60629-1
Chinese Journal of Natural Medicines

•Original article•

New pimarane diterpenoids with antibacterial activity from fungus *Arthrinium* sp. ZS03

ZHAO Songfeng, JING Ziwei*

Department of Pharmacy, the First Affiliated Hospital of Zhengzhou University, Zhengzhou 450052, China

Available online 20 Apr., 2024

[ABSTRACT] A comprehensive chemical study of the endophytic fungus *Arthrinium* sp. ZS03, associated with *Acorus tatarinowii* Schott, yielded eleven pimarane diterpenoids (compounds **1**–**11**), including seven novel compounds designated arthrinoids A–G (**1**–**7**). The determination of their structures and absolute configurations was achieved through extensive spectroscopic techniques, quantum chemical calculations of electronic circular dichroism (ECD), and single-crystal X-ray diffraction analysis. Furthermore, **7** demonstrated inhibitory activity against *Klebsiella pneumoniae*, comparable to the reference antibiotic amikacin, with a minimum inhibitory concentration (MIC) of 8 μg·mL^{-1}.

[KEY WORDS] *Arthrinium* sp. ZS03; Pimarane diterpenoids; Structural elucidation; Antibacterial activity
[CLC Number] R284.1 **[Document code]** A **[Article ID]** 2095-6975(2024)04-0356-09

Introduction

Endophytic fungi, ubiquitous within plant tissues, form significant mutualistic relationships with their hosts [1]. The quest to uncover structurally unique and bioactive natural products, along with elucidating the symbiotic relationships between plants and their endophytic microbes, has garnered widespread interest among biologists and chemists globally [2–4]. *Acorus tatarinowii* Schott, belonging to the Araceae family, is utilized in Traditional Chinese Medicine (TCM) for treating conditions such as forgetfulness, dementia, and stroke [5]. Despite its medicinal value, research on fungi derived from this plant has been limited. However, existing literature highlights that endophytic fungi from medicinal plants are prolific sources of novel, bioactive compounds [6–15], motivating our investigation into an endophytic fungus, *Arthrinium* sp. ZS03, isolated from *A. tatarinowii*. This investigation led to the identification of seven novel pimarane diterpenoids, termed arthrinoids A–G (**1**–**7**), alongside four previously identified compounds (**8**–**11**). This paper reports the isolation, structural elucidation, and antibacterial efficacy of these newly discovered diterpenoids (Fig. 1) .

[Received on] 29-Jul.-2023
[Research funding] This work was supported by the National Natural Science Foundation of China (No. 82003956) and the Henan Young Elite Scientists Sponsorship Program (No. 2023HYTP032).
[*]**Corresponding author]** E-mail: jingziwei1988@126.com
These authors have no conflict of interest to declare.

Results and Discussion

Compound **1** was isolated as a colorless block crystal. Its molecular formula was established as $C_{20}H_{26}O_5$, based on high-resolution electrospray ionization mass spectrometry (HR-ESI-MS) data, indicating eight degrees of unsaturation. The proton nuclear magnetic resonance (^{1}H NMR) data for **1** (Table 1) revealed the presence of four singlet methyl groups at δ_H 1.01 (3H, s, H_3-17), 1.13 (3H, s, H_3-20), 1.50 (3H, s, H_3-18), and 1.52 (3H, s, H_3-19). The ^{13}C NMR (Table 2) and distortionless enhancement by polarization transfer (DEPT) spectra exhibited twenty carbon signals, corresponding to four methyls (δ_C 19.8, 21.5, 22.7, and 24.9), five aliphatic methylenes (δ_C 23.8, 24.3, 30.7, 33.6, and 72.0), two oxygenated methines (δ_C 77.9 and 80.4), and seven quaternary carbons, which included four olefinic carbons (δ_C 128.5, 139.9, 144.7, and 167.5), and two keto carbonyl carbons (δ_C 181.9 and 216.8). Comparison of the one-dimensional (1D) NMR data (Tables 1 and 2) for **1** with those of the known pimarane diterpenoid pedinophyllol K (**9**) [16], whose absolute structure was determined by crystallography, highlighted a significant difference: the carbon at C-17 resonated at δ_C 19.8 in **1**, as opposed to δ_C 14.9 in **9**, suggesting that **1** and **9** are C-15 epimers. The planar structure of **1** was conclusively established through ^{1}H–^{1}H correlation spectroscopy (COSY) and heteronuclear multiple-bond correlation (HMBC) analyses (Fig. 2).

The nuclear overhauser effect spectroscopy (NOESY) correlations (Fig. 3) further elucidated the relative configuration of compound **1**. Correlations from H-11b (δ_H 2.35) to H_3-

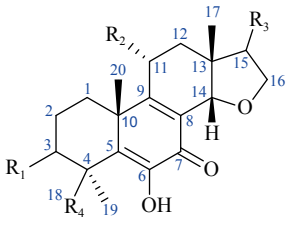

	R_1	R_2	R_3	R_4
1	=O	H	*α*-OH	CH_3
2	H	H	*α*-OH	CH_3
3	H	H	*α*-OH	CH_2OH
5	H	=O	*β*-OH	CH_3
6	H	*α*-OH	*β*-OH	CH_3
8	H	H	*β*-OH	CH_3
9	=O	H	*β*-OH	CH_3

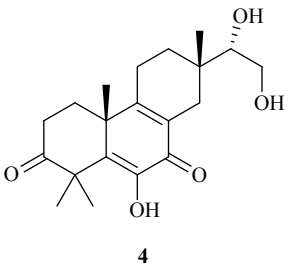

4

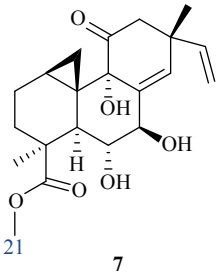

7

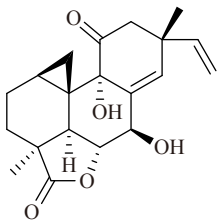

10

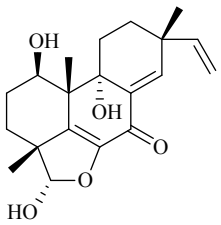

11

Fig. 1 Chemical structures of compounds 1–11.

17 (δ_H 1.01) and H_3-20 (δ_H 1.13), along with those from H-15 (δ_H 4.24) to H-14 (δ_H 4.42) and H_3-17 (δ_H 1.01), indicated the relative stereochemistry of **1** to be 10*R**,13*R**,14*S**,15*S**. To determine the absolute configuration, a high-quality crystal of **1**, obtained from acetone underwent single-crystal X-ray diffraction analysis using using Cu K*α* radiation (Fig. 4). The Flack parameter, determined to be –0.01(5) (CCDC reference 2173443), confirmed the absolute configuration as 10*R*,13*R*,14*S*,15*S*. Consequently, the structure of **1** was established and named arthrinoid A.

Compound **2** was obtained as a colorless oil. The HR-ESI-MS data established its molecular formula as $C_{20}H_{28}O_4$, which indicates seven degrees of unsaturation. The ^{1}H and ^{13}C NMR data (Tables 1 and 2) of **2** closely resembled those of **1**, with the primary difference being the substitution of the C-3 keto carbonyl (δ_C 216.8 in **1**) for a methylene group (δ_C 37.5) at the same position in **2**. This modification was corroborated by key HMBC interactions from H_3-18 (δ_H 1.38) to C-3 (δ_C 37.5), C-4 (δ_C 36.0), C-5 (δ_C 141.4), and C-19 (δ_C 27.7) (Fig. 2). The NOESY correlations (Fig. 3) and electronic circular dichroism (ECD) spectra (Fig. 5) of **1** and **2** were similar, leading to the conclusion that **2** also has the absolute configuration of 10*R*,13*R*,14*S*,15*S*. Consequently, the structure of **2** was elucidated and designated as arthrinoid B.

Compound **3** was obtained as a colorless oil, with a molecular formula of $C_{20}H_{28}O_5$ determined through HR-ESI-MS analysis. The 1D NMR spectra of **3** (Tables 1 and 2) closely resembled those of **2**, except for an additional hydroxyl group at C-18 (δ_C 68.8). This modification was supported by key HMBC correlations (Fig. 2) from H_2-18 (δ_H 3.61 and 4.08) to C-3 (δ_C 31.6), C-4 (δ_C 43.2), C-5 (δ_C 140.3), and C-19 (δ_C 22.5), indicating the presence of a hydroxymethyl group. Rotating frame Overhauser effect spectroscopy (ROESY) correlations were observed from (Fig. 3) from H-11b (δ_H 2.37) to H_3-17 (δ_H 0.99) and H_3-20 (δ_H 1.42), from H_3-20 (δ_H 1.42) to H-18b (δ_H 4.08), from H-12a (δ_H 1.68) to H-16a (δ_H 3.58), from H-12b (δ_H 1.60) to H_3-17 (δ_H 0.99), and from H-14 (δ_H 4.41) to H-15 (δ_H 4.22) and H-16b (δ_H 4.02), allowing the deduction of **3**'s relative configuration as 4*S**,10*R**,13*R**, 14*S**,15*S**. Similar ECD spectra (Fig. 5) between **3** and **1,** alongside a shared biogenetic origin, supported the assignment of the absolute configuration of **3** was 4*S*,10*R*,13*R*, 14*S*,15*S*. Consequently, this compound was identified and named arthrinoid C.

Compound **4** was isolated as a colorless oil. Its molecular formula, $C_{20}H_{28}O_5$, was established based on HR-ESI-MS data, indicating seven degrees of unsaturation. The ^{1}H NMR spectrum (Table 1) of **4** displayed four singlet methyl signals at δ_H 0.87 (3H, s, H_3-17), 1.12 (3H, s, H_3-20), and 1.50 (6H, s, H_3-18 and H_3-19). The ^{13}C NMR data (Table 2), analyzed with the assistance of DEPT and heteronuclear single quantum coherence (HSQC) spectra, identified twenty carbon signals. These included four methyls (δ_C 20.1, 21.5, 23.1, and 24.9), six aliphatic methylenes (δ_C 23.5, 30.3, 31.0, 32.8, 33.6, and 63.9), one oxygenated methine (δ_C 78.4), and seven quaternary carbons, of which four were olefinic (δ_C 129.1, 139.8, 144.3, and 162.7), and two were keto carbonyls (δ_C 182.7 and 217.2). A comparative analysis of 1D NMR data (Tables 1 and 2) for **4** and **1** suggested that both compounds share the same carbon skeleton but differ in the structural arrangement at the tetrahydrofuran ring present in **1**, which is open in **4**. This change resulted in the chemical shift of C-14 moving from δ_C 77.9 in **1** to δ_C 32.8 in **4**, indicating the ring opening. This modification was further corroborated by ^{1}H–^{1}H COSY and HMBC correlations as shown in Fig. 2, in addition to a reduction of one degree of unsaturation in **4**

Table 1 ^{1}H NMR data for compounds **1**–**7** (δ in ppm, J in Hz)

No.	**1** [a,c]	**2** [b,c]	**3** [a,d]	**4** [a,d]	**5** [b,c]	**6** [a,c]	**7** [a,c]
1	2.40, m; 1.87, m	1.94, m; 1.63, m	2.10, ddd (13.8, 9.3, 5.1); 1.56, m	2.36, m; 1.79, dd (13.5, 9.4)	2.44, m; 1.61, m	2.41, m; 1.64, m	1.14, m
2	2.85, m; 2.61, m	1.84, m; 1.64, m	1.93, m; 1.77, m	2.60, m;	1.84, m; 1.61, m	1.93, m; 1.75, m	1.89, m; 1.58, m
3		1.88, m; 1.38, m	1.33, m; 2.28, m		1.94, td (13.0, 5.3); 1.42, m	1.84, m; 1.80, m	1.67, m; 1.28, m
5							2.55, d (11.0)
6							3.75, dd (11.0, 9.1)
7							4.18, dd (9.1, 2.2)
11	2.67, m; 2.35, m	2.63, m; 2.29, m	2.67, ddd (19.2, 5.4, 3.1); 2.37, ddd (19.2, 11.5, 5.7)	2.53, m; 2.36, m		4.72, t (4.0)	
12	1.71, m; 1.61, m	1.75, m; 1.60, m	1.68, m; 1.60, m	1.73, ddd (13.6, 8.3, 5.6); 1.58, m	2.56, d (14.1); 2.21, dd (14.1, 1.2)	1.64, m; 1.44, m	2.58, d (13.2); 2.37, dd (13.2, 1.7)
14	4.42, s	4.48, s	4.41, s	2.36, m; 2.18, m	4.80, s	4.62, s	5.89, t (1.9)
15	4.24, dd (7.8, 7.3)	4.29, dd (7.6, 6.9)	4.22, dd (7.9, 7.2)	3.38, dd (8.6, 2.7)	3.96, dd (4.9, 1.8)	3.87, dd (5.3, 2.7)	5.65, dd (17.3, 10.4)
16	4.04, dd (8.7, 7.8); 3.60, dd (8.7, 7.3)	4.17, dd (9.0, 7.6); 3.66, dd (9.0, 6.9)	4.02, dd (8.7, 7.9); 3.58, dd (8.7, 7.2)	3.75, dd (11.2, 2.7); 3.52, dd (11.2, 8.6)	4.44, dd (10.3, 4.9); 3.92, dd (10.3, 1.8)	4.11, dd (9.7, 5.3); 3.63, dd (9.7, 2.7)	4.95, dd (17.3, 1.1); 4.89, dd (10.4, 1.1)
17	1.01, s	1.00, s	0.99, s	0.87, s	1.12, s	1.18, s	1.27, s
18	1.50, s	1.38, s	4.08, d (10.7); 3.61, d (10.7)	1.50, s	1.41, s	1.40, s	
19	1.52, s	1.37, s	1.34, s	1.50, s	1.39, s	1.40, s	1.40, s
20	1.13, s	1.40, s	1.42, s	1.12, s	1.61, s	1.64, s	0.99, t (6.1); 0.22, ddd (9.6, 6.5, 1.4)
21							3.65, s

[a] Recorded in methanol-d_4; [b] Recorded in chloroform-d; [c] Recorded at 400 MHz; [d] Recorded at 600 MHz; "m" means overlapped or multiplet with other signals.

Table 2 ^{13}C NMR data for compounds 1–7 (δ in ppm)

No.	1 [a,c]	2 [b,c]	3 [a,d]	4 [a,d]	5 [b,c]	6 [a,c]	7 [a,c]
1	30.7, CH_2	31.7, CH_2	31.5, CH_2	30.3, CH_2	29.2, CH_2	31.9, CH_2	15.9, CH
2	33.6, CH_2	17.8, CH_2	17.3, CH_2	33.6, CH_2	17.4, CH_2	18.6, CH_2	20.5, CH_2
3	216.8, C	37.5, CH_2	31.6, CH_2	217.2, C	36.6, CH_2	40.0, CH_2	34.9, CH_2
4	49.5, C	36.0, C	43.2, C	49.6, C	36.5, C	36.9, C	44.3, C
5	139.9, C	141.4, C	140.3, C	139.8, C	146.2, C	144.7, C	45.6, CH
6	144.7, C	144.2, C	146.1, C	144.3, C	145.4, C	145.6, C	78.7, CH
7	181.9, C	180.6, C	181.9, C	182.7, C	181.5, C	182.9, C	75.8, CH
8	128.5, C	125.4, C	126.7, C	129.1, C	136.2, C	128.5, C	140.9, C
9	167.5, C	169.2, C	171.5, C	162.7, C	155.9, C	167.5, C	78.0, C
10	43.6, C	43.2, C	44.1, C	43.1, C	42.3, C	44.9, C	29.1, C
11	23.8, CH_2	22.6, CH_2	23.8, CH_2	23.5, CH_2	198.8, C	65.0, CH	211.7, C
12	24.3, CH_2	23.3, CH_2	24.3, CH_2	31.0, CH_2	46.3, CH_2	40.0, CH_2	54.4, CH_2
13	42.1, C	41.0, C	42.0, C	35.4, C	48.1, C	43.1, C	43.2, C
14	77.9, CH	76.5, CH	78.0, CH	32.8, CH_2	74.3, CH	77.1, CH	129.0, CH
15	80.4, CH	80.3, CH	80.4, CH	78.4, CH	78.6, CH	79.5, CH	144.8, CH
16	72.0, CH_2	71.6, CH_2	71.9, CH_2	63.9, CH_2	76.2, CH_2	75.1, CH_2	113.6, CH_2
17	19.8, CH_3	19.8, CH_3	19.9, CH_3	20.1, CH_3	16.1, CH_3	17.7, CH_3	28.7, CH_3
18	21.5, CH_3	27.9, CH_3	68.8, CH_2	21.5, CH_3	27.7, CH_3	27.7, CH_3	179.7, C
19	24.9, CH_3	27.7, CH_3	22.5, CH_3	24.9, CH_3	27.2, CH_3	29.9, CH_3	30.8, CH_3
20	22.7, CH_3	31.0, CH_3	29.7, CH_3	23.1, CH_3	29.4, CH_3	32.8, CH_3	11.4, CH_2
21							52.1, CH_3

[a] Recorded in methanol-d_4; [b] Recorded in chloroform-d; [c] Recorded at 100 MHz; [d] Recorded at 150 MHz.

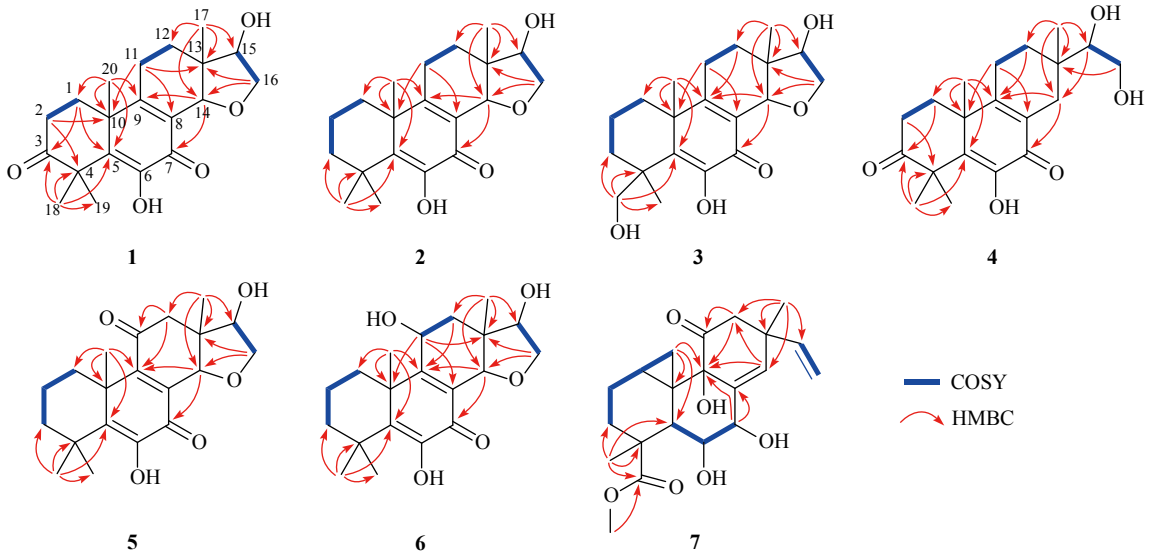

Fig. 2 Selected ^{1}H–^{1}H COSY and HMBC correlations of compounds 1–7.

compared to **1**, as evidenced by the HR-ESI-MS data **4**.

The relative configuration of **4** was elucidated through the analysis of rotating frame ROESY data (Fig. 3). The ROESY correlations from H-11b (δ_H 2.36) to H_3-17 (δ_H 0.87) and H_3-20 (δ_H 1.12) indicated that H_3-17 and H_3-20 both adopted a β-orientation. The absolute configuration of the 15,16-

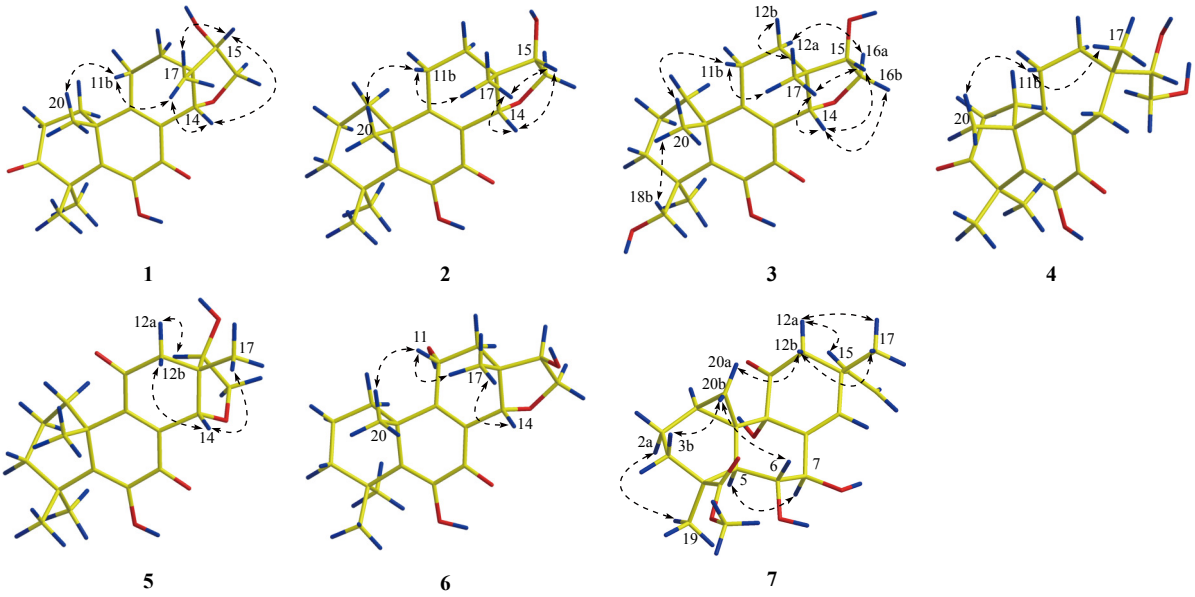

Fig. 3 Key NOESY/ROESY correlations of compounds 1–7.

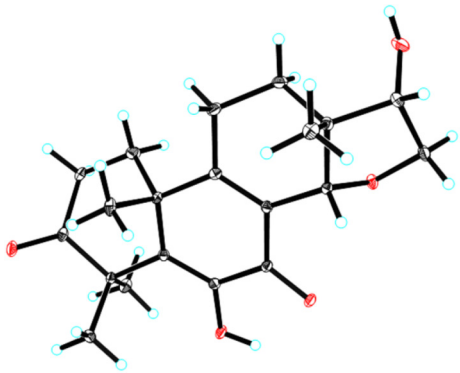

Fig. 4 ORTEP drawing of compound 1.

diol motif in **4** was edetermined using the in situ dimolybdenum circular dichroism (CD) method [17]. Upon addition of **4** to $Mo_2(AcO)_4$ in dimethyl sulfoxide (DMSO), the resulting metal complex exhibited a positive Cotton effect at approximately 310 nm (Fig. 6), consistent with a 15*S*-configuration according to the empirical helicity rule, which relates the sign of the Cotton effect of the diagnostic O–C–C–O moiety [18] to its configuration. Given the common biogenetic origin with the pimarane diterpenoid framework, the absolute configuration of **4** was postulated as 10*R*,13*S*,15*S*. This hypothesis was subsequently confirmed by comparing the experimented and calculated ECD curves (Fig. 5). Thus, the structure of **4** was conclusively identified and designated as arthrinoid D.

Compound **5** was obtained as a colorless oil, with its molecular formula established as $C_{20}H_{26}O_5$ based on HR-ESI-MS data. A comparative analysis of the 1D NMR spectra (Tables 1 and 2) of **5** and **9** srevealed a notable difference: the carbonyl carbon at C-3 in **9** (δ_C 216.9) was replaced a carbonyl by at C-11 (δ_C 198.8) in **5**. This observation was corroborated by key the HMBC correlations (Fig. 2) from H_3-18 (δ_H 1.41) to C-3 (δ_C 36.6), C-4 (δ_C 36.5), C-5 (δ_C 146.2), and C-19 (δ_C 27.2) and from H_2-12 (δ_H 2.21 and 2.56) to C-11 (δ_C 198.8), thereby elucidating the relative structure of **5**. Given the common biogenetic pathway and similar NOESY data (Fig. 3) between **5** and **9**, along with supportive experimental and calculated ECD spectra (Fig. 5), the absolute configuration of **5** was determined to be 10*R*,13*R*,14*S*,15*R*. Consequently, this compound was identified and named arthrinoid E.

Compound **6** was obtained as a colorless oil, with the molecular formula $C_{20}H_{28}O_5$, established through HR-ESI-MS analysis. The ^{1}H and ^{13}C NMR spectra (Tables 1 and 2) of **6** were nearly identical to those of **5**, with the significant distinction being the replacement of the C-11 keto carbonyl group (δ_C 198.8 in **5**)was replaced by an sp^3-hybridized methine (δ_C 65.0) at the same position in **6**. This structural modification was confirmed by HMBC correlations (Fig. 2) from H-11 (δ_H 4.72) to C-8 (δ_C 128.5), C-9 (δ_C 167.5), C-10 (δ_C 44.9), C-12 (δ_C 40.0), and C-13 (δ_C 43.1). Critical NOESY correlations (Fig. 3) notably between H-11 (δ_H 4.72) and H_3-20 (δ_H 1.64), combined with the shared biogenetic pathway and comparable ECD spectra (Fig. 5) between **6** and **5**, indicated that **6** possesses the absolute configuration of 10*R*,11*R*,13*R*,14*S*,15*R*. Thus, the structure of **6** was elucidated and designated as arthrinoid F.

Compound **7** was isolated as a colorless oil, its molecular formula, $C_{21}H_{28}O_6$, was determined through HR-ESI-MS data. ^{1}H NMR analysis (Table 1) revealed four olefinic protons at H-14 (δ_H 5.89), H-15 (δ_H 5.65), H-16a (δ_H 4.89), and H-16b (δ_H 4.95) along with a cyclopropyl group represented by H_2-20 (δ_H 0.99 and 0.22). ^{13}C NMR data (Table 2) identified the presence of a carbonyl carbon at C-11 (δ_C 211.7), an ester carbonyl carbon at C-18 (δ_C 179.7), and three methyl carbons at C-17 (δ_C 28.7), C-19 (δ_C 30.8), and C-21 (δ_C 52.1).

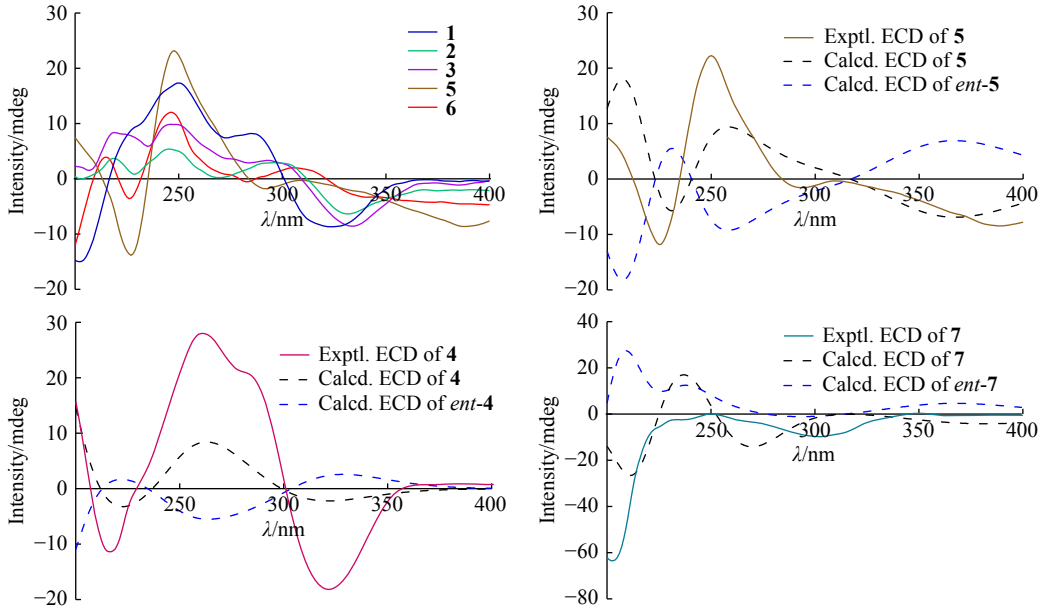

Fig. 5 Experimental ECD curves of 1–3 and 5–6 and comparison of calculated and experimental ECD curves of 4, 5, and 7 in MeOH.

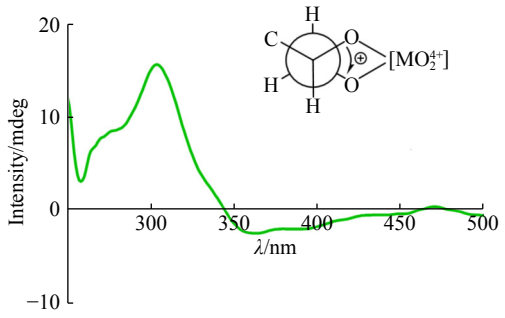

Fig. 6 $[Mo_2(OAc)_4]$-induced ICD spectrum of 4 in DMSO.

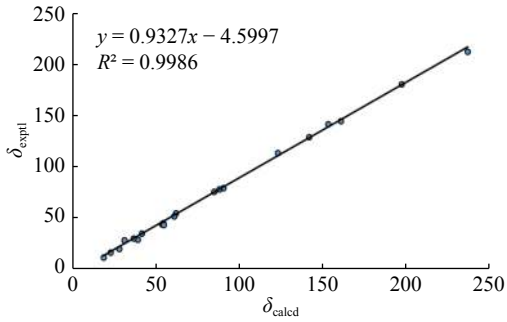

Fig. 7 Linear correlation between the experimental and calculated ^{13}C NMR chemical shifts for 7.

Comparing the 1D NMR data (Tables 1 and 2) of **7** with those of myrocin D (**10**) [19] revealed the primary difference to be the opening of the five-membered lactone ring in **10** and the addition of a methoxy group (δ_C 52.1, C-21) in **7**. This structural variation was supported by HMBC (Fig. 2) from H_3-21 (δ_H 3.65) to C-18. The relative configuration of **7** was elucidated through the analysis of NOESY data (Fig. 3). Notable NOE correlations from H-20b (δ_H 0.99) to H-6 (δ_H 3.75) and H-3b (δ_H 1.67), from H-2a (δ_H 1.89) to H_3-19 (δ_H 1.40), from H-5 (δ_H 2.57) to H-7 (δ_H 4.18) and H_3-19 (δ_H 1.40), from H-12b (δ_H 2.58) to H-20a (δ_H 0.22), and from H-12a (δ_H 2.37) to H-15 indicated β-orientations for H-6, H_2-20, and H_3-17, while α-orientations were deduced for H-5, H-7, H_3-19, and OH-9. Significant coupling constants between H-5/H-6 and H-6/H-7 (11.0 and 9.1 Hz, respectively) suggested trans-relationships, corroborating the deduced relative configurations for C-5, C-6, and C-7. The structure of **7** further validated by a comparison of experimental and calculated ^{13}C NMR data, which showed an R^2 value of 0.9986 (Fig. 7). affirming the relative configuration (Fig. 5). The absolute configuration of **7** was determined to be 1*S*,4*S*,5*R*,6*R*,7*R*,9*S*, 10*S*,13*R*. through analysis of calculated ECD data, leading to the naming of this compound as arthrinoid G.

Four known compounds were identified through comparison of their NMR and HR-ESI-MS data with literature values: pedinophyllol L (**8**) [16], pedinophyllol K (**9**) [16], both previously reported in reference 16, as well as myrocin D (**10**) [19], and libertellenone E (**11**) [19].

The newly isolated compounds **1**–**7** were assessed for their antibacterial efficacy against a panel of microbial pathogens, including *Escherichia coli*, *Pseudomonas aeruginosa*, *Klebsiella pneumoniae*, and *Acinetobacter baumannii*. These evaluations revealed that all new compounds demonstrated varying levels of inhibitory activity. Notably, **7** displayed inhibitory activity against *K. pneumoniae* comparable to that of the reference antibiotic amikacin, with a minimum inhibitory concentration (MIC) value of 8 μg·mL^{-1} (Table 3).

Experimental

General experimental procedures

Optical rotations were determined using a PerkinElmer

Table 3 Antibacterial activities of compounds 1–7

Compounds	MIC/(μg·mL^{-1})			
	E. coli	*P. aeruginosa*	*K. pneumoniae*	*A. baumannii*
1	≥ 100	32	≥ 100	≥ 100
2	≥ 100	64	≥ 100	≥ 100
3	32	≥ 100	16	32
4	64	64	32	≥ 100
5	≥ 100	≥ 100	≥ 100	32
6	32	32	64	≥ 100
7	16	64	8	64
Amikacin	4	2	8	2

PE-341 polarimeter. Ultraviolet (UV) spectra were obtained with a PerkinElmer Lambda 35 spectrophotometer. CD experimental data were collected on a JASCO-810 spectrometer. Infrared (IR) spectra were recorded using a Tenor 27 FT-IR spectrometer with potassium bromide (KBr) pellets. 1D (^{1}H, ^{13}C, and DEPT) and 2D (HSQC, ^{1}H–^{1}H COSY, HMBC, and NOESY/ROESY) NMR data were obtained on Bruker AM-400 or AM-600 NMR spectrometers, using tetramethylsilane (TMS) as the internal standard. Chemical shifts (δ) were referenced to the solvent signals for methanol-d_4 (δ_H 3.31 and δ_C 49.0) and chloroform-*d* (δ_H 7.26 and δ_C 77.2). HR-ES-IMS data in the positive ion mode were recorded on a Thermo Fisher LC-LTQ-Orbitrap XL spectrometer. For column chromatography (CC), silica gel (100–200 and 200–300 mesh, Qingdao Marine Chemical, Inc., Qingdao, China), Sephadex LH-20 (GE Healthcare Bio-Sciences AB, Sweden), and Lichroprep RP-C_{18} gel (50 μm, YMC Co. Ltd., Japan) were utilized. Compounds were purified using an Agilent 1200 liquid chromatograph equipped with an RP-C_{18} column (5 μm, 10 mm × 250 mm, Welch Ultimate XB-C_{18}). Thin-layer chromatography (TLC) was performed on silica gel 60 F_{254} plates (Yantai Chemical Industry Research Institute, Yantai, China), and spots were visualized by heating the plates after application of a 10% sulfuric acid (H_2SO_4) in in ethanol (EtOH) solution.

Fungal material

Strain *Arthrinium* sp. ZS03 was isolated from the rhizome of *Acorus tatarinowii* Schott, collected in Zhengzhou City in September 2018. A voucher specimen (ZSF20180912) is preserved in the Department of Pharmacy at the First Affiliated Hospital of Zhengzhou University.

Extraction and isolation

The strain *Arthrinium* sp. ZS03 was cultivated on potato dextrose agar (PDA) at 28 °C for 7 d to establish seed cultures. Subsequently, agar plugs were sectioned into small pieces and transferred to 100 Erlenmeyer flasks (1 L each), containing 200 g of rice and 250 mL of distilled water. These setups were sterilized *via* autoclaving and incubated at 28 °C for 30 d. Post-incubation, the fermented rice was extracted with 95% EtOH eight times. The EtOH was then evaporated under reduced pressure, yielding a residue. This residue was suspended in water and partitioned with ethyl acetate (EtOAc). The EtOAc layer was collected, and the organic solvent was removed to obtain a crude extract (287 g).

The crude EtOAc extract (287 g) underwent silica gel CC utilizing a gradient elution system of petroleum ether (PE)–EtOAc (ranging from 20 ∶ 1 to 0 ∶ 1, *V*/*V*), resulting in five principal fractions (A–E). Fraction D (65 g) was fractionated by further divided by reverse-phase C_{18} (RP-C_{18}) silica gel CC, eluted with methanol (MeOH)–water (H_2O) gradients (20% to 100%), producing five subfractions (D1–D5). Subfraction D3 (3.7 g) was then processed using Sephadex LH-20 chromatography (dichloromethane (CH_2Cl_2)–MeOH, 1 ∶ 1, *V*/*V*), yielding four subfractions (D3-1–D3-4). Subfraction D3-2 (200 mg) underwent semipreparative RP-C_{18} high-performance liquid chromatography (HPLC) (acetonitrile (MeCN–H_2O, 60 ∶ 40, 2.0 mL·min^{-1}) to isolate **7** (5 mg, t_R = 28 min). Subfraction D3-3 (1 g) was purified using silica gel CC (PE–EtOAc gradient from 20 ∶ 1–1 ∶ 1, *V*/*V*), and refined by semipreparative RP-C_{18} HPLC (MeCN–H_2O, 61 ∶ 39, *V*/*V*; 2.0 mL·min^{-1}) to yield **2** (2.2 mg, t_R = 28 min) and **8** (25 mg, t_R = 40 min). Fraction E (61 g) was fractionated on an octadecylsilane (ODS) column using MeOH–H_2O (20%–100%) gradient, separating it into five subfractions (E1–E5). Subfraction E2 (3.9 g) underwent silica gel CC (PE–EtOAc gradient from 20 ∶ 1–1 ∶ 1, *V*/*V*), resulting in four main subfractions (E2-1–E2-4). Subfraction E2-4 was further purified using Sephadex LH-20 (CH_2Cl_2–MeOH, 1 ∶ 1, *V*/*V*) and semipreparative RP-C_{18} HPLC (MeCN–H_2O, 45 ∶ 55, *V*/*V*; flow rate: 2.0 mL·min^{-1}) to yield **4** (1.5 mg, t_R = 22 min), **6** (4.1 mg, t_R = 40 min), and **11** (22 mg, t_R = 32 min). Subfraction E3 (800 mg) was fractionated *via* Sephadex LH-20 (CH_2Cl_2–MeOH, 1 ∶ 1, *V*/*V*) and silica gel CC (PE–EtOAc, gradient from 10 ∶ 1–1 ∶ 1, *V*/*V*), resulting in two subfractions (E3-1–E3-2), Subfraction E3-1 was purified by semipreparative RP-C_{18} HPLC (MeOH–H_2O, 58 ∶ 42, *V*/*V*; 2.0 mL·min^{-1}) to obtain compounds **5** (3 mg, t_R = 42 min) and **10** (1.5 mg, t_R = 21 min). Finally, subfraction E3-2

was refined using semipreparative RP-C_{18} HPLC (MeCN–H_2O, 37 : 63, *V/V*; low rate: 2.0 mL·min^{-1}) to isolate **1** (26 mg, t_R = 35 min), **3** (3 mg, t_R = 21 min), and **9** (15 mg, t_R = 23 min).

*Arthrinoid A (**1**)*: $C_{20}H_{26}O_5$; colorless block crystals; mp: 232–234 °C; $[\alpha]_D^{20}$: +99 (*c* 1.0, MeOH); UV (MeOH) λ_{max} (log ε): 208 (4.09), 253 (3.88), 300 (3.69) nm; IR (KBr) ν_{max}: 3383, 2971, 2935, 2876, 1711, 1634, 1422, 1363, 1252, 1114, 1025 cm^{-1}; ECD (MeOH) λ_{max} (mdeg, 0.25 mg·mL^{-1}): 250 (+17.36), 273 (+7.42), 285 (+8.21), 324 (–8.66), 371 (–0.15) nm; For ^{1}H and ^{13}C NMR data (Tables 1 and 2); HR-ESI-MS $[M + Na]^+$ *m/z* 369.1668 (Calcd. for $C_{20}H_{26}O_5Na^+$, 369.1672).

*Arthrinoid B (**2**)*: $C_{20}H_{28}O_4$; yellow oil; $[\alpha]_D^{20}$: +7 (*c* 1.0, MeOH); UV (MeOH) λ_{max} (log ε): 202 (3.73), 252 (3.53) nm; IR (KBr) ν_{max}: 3431, 2935, 1704, 1632, 1460, 1384, 1025 cm^{-1}; ECD (MeOH) λ_{max} (mdeg, 0.625 mg·mL^{-1}): 247 (+4.93), 269 (+0.34), 294 (+3.03), 332 (–6.18) nm; For ^{1}H and ^{13}C NMR data (Tables 1 and 2); HR-ESI-MS $[M + Na]^+$ *m/z* 355.1889 (Calcd. for $C_{20}H_{28}O_4Na^+$, 355.1880).

*Arthrinoid C (**3**)*: $C_{20}H_{28}O_5$; colorless oil; $[\alpha]_D^{20}$: –3 (*c* 1.0, MeOH); UV (MeOH) λ_{max} (log ε): 213 (3.50), 254 (3.32), 308 (3.06) nm; IR (KBr) ν_{max}: 3420, 2953, 2934, 2876, 1628, 1459, 1424, 1384, 1112, 1024 cm^{-1}; ECD (MeOH) λ_{max} (mdeg, 0.625 mg·mL^{-1}): 252 (+8.86), 333 (–7.97), 371 (–0.85) nm; For ^{1}H and ^{13}C NMR data (Tables 1 and 2); HR-ESI-MS $[M + Na]^+$ *m/z* 371.1832 (Calcd. for $C_{20}H_{28}O_5Na^+$, 371.1829).

*Arthrinoid D (**4**)*: $C_{20}H_{28}O_5$; colorless oil; $[\alpha]_D^{20}$: +26 (*c* 1.0, MeOH); UV (MeOH) λ_{max} (log ε): 202 (4.11), 258 (4.01), 301 (3.70) nm; IR (KBr) ν_{max}: 3479, 2975, 2935, 1710, 1624, 1609, 1424, 1383, 1244, 1084, 1020 cm^{-1}; ECD (MeOH) λ_{max} (mdeg, 0.50 mg·mL^{-1}): 217 (–11.35), 261 (+28.04), 322 (–18.16), 357 (+0.05) nm; For ^{1}H and ^{13}C NMR data (Tables 1 and 2); HR-ESI-MS $[M + Na + H]^{2+}$ *m/z* 372.1907 (Calcd. for $C_{20}H_{29}O_5Na^{2+}$, 372.1902).

*Arthrinoid E (**5**)*: $C_{20}H_{26}O_5$; colorless oil; $[\alpha]_D^{20}$: –23 (*c* 1.0, MeOH); UV (MeOH) λ_{max} (log ε): 231 (3.88), 267 (3.43) nm; IR (KBr) ν_{max}: 3403, 2957, 2931, 1690, 1634, 1597, 1459, 1425, 1383, 1374, 1273, 1216 cm^{-1}; ECD (MeOH) λ_{max} (mdeg, 0.50 mg·mL^{-1}): 225 (–11.83), 250 (+22.25), 294 (–1.56) nm; For ^{1}H and ^{13}C NMR data (Tables 1 and 2); HR-ESI-MS $[M + Na]^+$ *m/z* 369.1664 (Calcd. for $C_{20}H_{26}O_5Na^+$, 369.1672).

*Arthrinoid F (**6**)*: $C_{20}H_{28}O_5$; colorless oil; $[\alpha]_D^{20}$: –12 (*c* 1.0, MeOH); UV (MeOH) λ_{max} (log ε): 201 (3.92), 228 (3.84), 328 (3.14) nm; IR (KBr) ν_{max}: 3400, 2956, 2933, 1690, 1633, 1597, 1384, 1217 cm^{-1}; ECD (MeOH) λ_{max} (mdeg, 0.50 mg·mL^{-1}): 246 (+10.72), 286 (–0.12), 308 (+1.92) nm; For ^{1}H and ^{13}C NMR data (Tables 1 and 2); HR-ESI-MS $[M + Na]^+$ *m/z* 371.1836 (Calcd. for $C_{20}H_{28}O_5Na^+$, 371.1829).

*Arthrinoid G (**7**)*: $C_{21}H_{28}O_6$; colorless oil; $[\alpha]_D^{20}$: –89 (*c* 1.0, MeOH); UV (MeOH) λ_{max} (log ε): 202 (3.74) nm; IR (KBr) ν_{max}: 3456, 2957, 2932, 1713, 1384, 1139, 1055, 925 cm^{-1}; ECD (MeOH) λ_{max} (mdeg, 0.57 mg·mL^{-1}): 203 (–63.49), 251 (+0.02), 302 (–9.71), 344 (–0.06) nm; For ^{1}H and ^{13}C NMR data (Tables 1 and 2); HR-ESI-MS $[M + Na]^+$ *m/z* 399.1808 (Calcd. for $C_{21}H_{28}O_6Na^+$, 399.1778).

X-ray crystal structure analysis

A suitable crystal of compound **1** was obtained through the slow evaporation of MeOH at room temperature. X-ray crystallographic analysis was performed using a Bruker APEX DUO diffractometer equipped with Cu Kα radiation. The structure was solved *via* direct methods using the Olex2 software and refined anisotropically with the SHELXL-2014/7 refinement package, employing full-matrix least-squares on F^2 [20–24]. Anisotropic displacement parameters were applied to all non-hydrogen atoms, and hydrogen atoms were placed in calculated positions and refined using a riding model. Crystallographic data for **1** have been deposited in the Cambridge Crystallographic Data Centre (CCDC 2173443). Copies of this data are available free of charge upon request to the CCDC, located at 12 Union Road, Cambridge CB 1EZ, UK [Fax: Int. + 44 (0) (1223) 336 033; e-mail: deposi@ccdc.cam.ac.uk].

*Crystal data for **1***: $C_{20}H_{26}O_5$, M = 346.41, a = 8.0686(2) Å, b = 10.0105(3) Å, c = 20.9046(5) Å, α = 90°, β = 90°, γ = 90°, V = 1688.48(8) Å^3, T = 100(2) K, space group $P2_12_12_1$, Z = 4, μ(Cu Kα) = 0.790 mm^{-1}, 14385 reflections measured, 3203 independent reflections (R_{int} = 0.0488). The final R_1 values were 0.0273 ($I > 2\sigma(I)$). The final $wR(F^2)$ values were 0.0690 ($I > 2\sigma(I)$). The final R_1 values were 0.0289 (all data). The final $wR(F^2)$ values were 0.0698 (all data). The goodness of fit on F^2 was 1.070. Flack parameter = –0.01(5).

ECD calculations

The optimized structures of compounds **4**, **5**, and **7** were generated using the BALLOON software and further refined through semiempirical PM3 quantum mechanical geometry optimizations employing the Gaussian 09 software suite [25]. The process of conformation optimization, ECD data calculation, and the final combination ECD spectra adhered to methodologies outlined in prior literature [25].

^{13}C NMR calculations

Conformational analysis of compound **7** was performed using a random search method in Sybyl-X 2.0, applying the MMFF94S force field with an energy cutoff of 2.5 kcal·mol^{-1}. This analysis identified nine lowest energy conformers for **7**. These conformers were then subjected to geometry optimizations and frequency analyses employing density functional theory (DFT) at the B3LYP-D3(BJ)/6-31G* level in in the polarizable continuum model (PCM) for methanol, using the Gaussian 09 software package. Each conformer was confirmed to be a stable point on the potential energy surface (PES), evidenced by the absence of imaginary frequencies. NMR shielding constants were calculated using the gauge-including atomic orbital (GIAO) method at the B972/pcSseg-2 level in PCM methanol, also with Gaussian 09. Gibbs free energies for the conformers were determined utilizing thermal correction at the B3LYP-D3(BJ)/6-31G* level with Gaussian 09, while electronic energies were evalu-

ated at the wB97M-V/def2-TZVP level in the solvation model density (SMD) for methanol using ORCA5.0.0 software. To obtain the final NMR chemical shifts, the chemical shifts of the conformers were averaged based on the Boltzmann distribution theory, considering their relative Gibbs free energies (ΔG).

$[Mo_2(OAc)_4]$-induced circular dichroism

To prepare the stock solution, $[Mo_2(OAc)_4]$ (1 mg) was dissolved in DMSO (1 mL). Following this, **4** (0.5 mg) was added to the solution. The CD spectrum was recorded immediately after the addition of **4** to the solution, and subsequent scans were performed at 10-minute intervals over a 30-minute period. This procedure ultimately yielded the stationary CD spectrum induced by $[Mo_2(OAc)_4]$, providing valuable insights into the chiral properties of **4** when complexed with the molybdenum acetate dimer in a DMSO solution.

Antibacterial activity assay

The minimum inhibitory concentrations (MICs) of **1**–**7** against four bacterial strains, *E. coli*, *P. aeruginosa*, *K. pneumoniae*, and *A. baumannii*, were determined using the broth microdilution method as previously described [26–28].

References

[1] Kusari S, Spiteller M. Are we ready for industrial production of bioactive plant secondary metabolites utilizing endophytes? [J]. *Nat Prod Rep*, 2011, **28**(7): 1203-1207.

[2] Kusari S, Hertweck C, Spiteller M. Chemical ecology of endophytic fungi: origins of secondary metabolites [J]. *Chem Biol*, 2012, **19**(7): 792-798.

[3] Kusari S, Pandey SP, Spiteller M. Untapped mutualistic paradigms linking host plant and endophytic fungal production of similar bioactive secondary metabolites [J]. *Phytochemistry*, 2013, **91**: 81-87.

[4] Wang WX, Kusari S, Laatsch H, *et al*. Antibacterial azaphilones from an endophytic fungus, *Colletotrichum* sp. BS4 [J]. *J Nat Prod*, 2016, **79**(4): 704-710.

[5] Gao E, Zhou ZQ, Zou J, *et al*. Bioactive asarone-derived phenylpropanoids from the rhizome of *Acorus tatarinowii* Schott [J]. *J Nat Prod*, 2017, **80**(11): 2923-2929.

[6] Ye K, Ai HL, Liu JK. Identification and bioactivities of secondary metabolites derived from endophytic fungi isolated from ethnomedicinal plants of Tujia in Hubei Province: a review [J]. *Nat Prod Bioprospect*, 2021, **11**: 185-205.

[7] Liu N, Song MN, Zhang QQ, *et al*. GKK1032B from endophytic *Penicillium citrinum* induces the apoptosis of human osteosarcoma MG63 cells through caspase pathway activation [J]. *Chin J Nat Med*, 2022, **20**(1): 67-73.

[8] Zhu JJ, Huang QS, Liu SQ, *et al*. Four new diphenyl ether derivatives from a mangrove endophytic fungus *Epicoccum sorghinum* [J]. *Chin J Nat Med*, 2022, **20**(7): 537-540.

[9] Gan D, Li C, Shu Y, *et al*. Steroids and dihydroisocoumarin glycosides from *Xylaria* sp. by the one strain many compounds strategy and their bioactivities [J]. *Chin J Nat Med*, 2023, **21**(2): 154-160.

[10] Li F, Ye Z, Huang Z, *et al*. New α-pyrone derivatives with herbicidal activity from the endophytic fungus *Alternaria brassicicola* [J]. *Bioorg Chem*, 2021, **117**: 105452.

[11] Wei PP, Ji JC, Ma XJ, *et al*. Three new pyrrole alkaloids from the endophytic fungus *Albifmbria viridis* [J]. *Nat Prod Bioprospect*, 2022, **12**: 5.

[12] Gao W, Chai C, He Y, *et al*. Periconiastone A, an antibacterial ergosterol with a pentacyclo[8.7. $0.0^{1,5}$. $0^{2,14}$. $0^{10,15}$]heptadecane system from *Periconia* sp. TJ403-rc01 [J]. *Org Lett*, 2019, **21**(20): 8469-8472.

[13] Hu Z, Ye Y, Zhang Y. Large-scale culture as a complementary and practical method for discovering natural products with novel skeletons [J]. *Nat Prod Rep*, 2021, **38**(10): 1775-1793.

[14] Peng X, Chang J, Gao Y, *et al*. Thiocytochalasins A−D, four sulfur-containing cytochalasans from an endophytic fungus *Phoma multirostrata* XJ-2-1 [J]. *Chin Chem Lett*, 2022, **33**(10): 4572-4576.

[15] Li F, Lin S, Zhang S, *et al*. Alterbrassinoids A–D: fusicoccane-derived diterpenoid dimers featuring different carbon skeletons from *Alternaria brassicicola* [J]. *Org Lett*, 2019, **21**(45): 8353-8357.

[16] Xu K, Zhang X, Chen JW, *et al*. Anti-inflammatory diterpenoids from an endophytic fungus *Phomopsis* sp. S12 [J]. *Tetrahedron Lett*, 2019, **60**(38): 151045.

[17] Guo LF, Liu GR, Liu L. Caryophyllene-type sesquiterpenoids and α-furanones from the plant endophytic fungus *Pestalotiopsis theae* [J]. *Chin J Nat Med*, 2020, **18**(4): 261-267.

[18] Górecki M, Jabłońska E, Kruszewska A, *et al*. Practical method for the absolute configuration assignment of *tert*/*tert* 1,2-diols using their complexes with $Mo_2(OAc)_4$ [J]. *J Org Chem*, 2007, **72**(8): 2906-2916.

[19] Tsukada M, Fukai M, Miki K, *et al*. Chemical constituents of a marine fungus, *Arthrinium sacchari* [J]. *J Nat Prod*, 2011, **74**: 1645-1649.

[20] Hu YL, Li XR, Xu G. Carascynol A, a hybrid of caryophyllane-type terpenoid and a C_6 unit degraded by polyprenylated acylphloroglucinols from *Hypericum ascyron* [J]. *Nat Prod Bioprospect*, 2022, **12**: 38.

[21] Zhang S, Mo S, Li F, *et al*. Drimane sesquiterpenoids from a wetland soil-derived fungus *Aspergillus calidoustus* TJ403-EL05 [J]. *Nat Prod Bioprospect*, 2022, **12**: 27.

[22] Hou L, Mei CX, Yuan CM, *et al*. Five new limonoids isolated from *Walsura robusta* [J]. *Nat Prod Bioprospect*, 2023, **13**(1): 7.

[23] Yang B, Su JC, Huang L, *et al*. Hyperispirones A and B, spiro-bridged polycyclic polyprenylated acylphloroglucinols with antiangiogenesis activity from *Hypericum beanii* [J]. *Org Chem Front*, 2022, **9**(13): 3460-3466.

[24] Wang L, Zhou Z, Huang JP, *et al*. Strepyrrolins A–E, five pyrrole-sesquiterpene hybrids from *Streptomyces* sp. KIB 015, revealing a new formation logic of pyrroles by isotope labeling [J]. *Org Chem Front*, 2023, **10**(4): 880-889.

[25] Song Y, Tan Y, She J, *et al*. Tanzawaic acid derivatives from the marine-derived *Penicillium steckii* as inhibitors of RANKL-induced osteoclastogenesis [J]. *J Nat Prod*, 2023, **86**: 1171-1178.

[26] Liu MT, Sun WG, Shen L, *et al*. Bipolarolides A–G, ophiobolin-derived sesterterpenes with three new carbon skeletons from *Bipolaris* sp. TJ403-B1 [J]. *Angew Chem Int Edit*, 2019, **58**: 12091-12095.

[27] Liu M, He Y, Shen L, *et al*. Bipolarins A–H, eight new ophiobolin-type sesterterpenes with antimicrobial activity from fungus *Bipolaris* sp. TJ403-B1 [J]. *Chin J Nat Med*, 2019, **17**(12): 935-944.

[28] Guo ZK, Zhu WY, Zhao LX, *et al*. New antibacterial depsidones from an ant-derived fungus *Spiromastix* sp. MY-1 [J]. *Chin J Nat Med*, 2022, **20**(8): 627-632.

Cite this article as: ZHAO Songfeng, JING Ziwei. New pimarane diterpenoids with antibacterial activity from fungus *Arthrinium* sp. ZS03 [J]. *Chin J Nat Med*, 2024, **22**(4): 356-364.